Powder Consideration For Additive Manufacturing Simulation

M. Dal[1], Y. Mayi[1], K. Marchais[2], P. Peyre[1]
1. Laboratoire Procédés et Ingénierie en Mécanique et Matériaux (PIMM) – UMR 8006, Arts et Metiers Institute of Technology, CNRS, CNAM, PIMM, HESAM Université, F-75013 Paris, France
2. Arts et Metiers Institute of Technology, University of Bordeaux, CNRS, Bordeaux INP, INRAE, I2M Bordeaux, Talence F-33400, France

Introduction

Additive manufacturing or metallic 3D printing is one of the current growing industrial technologies. As the heavy industry (energy, automotive, aircraft, …) is trying to master the processes to ensure pieces quality, a lot of experimental studies are appearing in the research field. Nevertheless, for powder bed technologies, experimental investigations illustrate some difficulties in terms of built instabilities or pores appearance. In this context, numerical approach can give some information and explanations.
Numerically, three point of views are mainly emerging in literature, i) the macroscopic analysis, mainly for thermomechanical studies of the whole piece [1] , ii) the microscopic analysis, for metal microstructures calculations [2] and iii) the mesoscopic analysis, for single track molten pool study.
As the process stability or instabilities is highly dependent of the elementary single-track quality, the mesoscale analysis is an interesting point of view. Moreover, as it is largely multiphysics (laser beam, heat transfers, fluid flows, …) and multiphase (bulk, powder, gas) it is also a complex case to be analyzed numerically. Thus, a common assumption found in the literature is the homogenization of the powder phase [3-5]. Nevertheless, this method is not able to simulate accurately the powder melting, coalescence or global powder behavior. Moreover, the equivalent thermal properties [6-7] assigned to the "powder phase" are strongly sensitive and very inaccurate in case of thin powder layer. Thus, some researchers have considered the whole particles of a part of the powder bed in their simulation [8]. The numerical problems considering the powder need strong computing resources and efficient numerical algorithms to be solved.
The COMSOL Multiphysics© software seems to be an efficient tool to investigate this field due to its capacity to threat multiphysical problems and its free boundary pre-implemented methods.

The Laser Powder Bed Fusion (LPBF) is a sequential process with a final workpiece built layer by layer. A "layer" is the spreading of a few micrometers of powder and this last is selectively molten by laser, track after track making a workpiece slice. Thus, the single-track quality has an effect horizontally on other tracks of the same layer and vertically on the next layer tracks. For instance, the main defects are pore generation due to local lack of powder (denudation) or particles aggregated on the bed (due to spatters) and drift of sample dimension due to flow instabilities or mechanical effects (not treated here). All of them can be related to single track quality.

In this paper, authors describe a mesoscale (single-track) model of LPBF able to simulate some process behavior and giving some process answers. After having justified several assumptions, the physical phenomena and numerical parameters will be described. Then, the results in terms of molten zones for several process parameters will be shown and discussed.

Theory and Assumptions

As author's investigations are made at the mesoscale (size of the molten pool), the considered phenomena are heat transfers, fluid flows and mass conservation. To these phenomena, the motion and the tracking of the metal-gas interface have to be added. In this particular case, the Phase Field Eulerian method has been chosen. As the LPBF process is mainly applied with very high feeding rates (around *1 m/s*) we assume a poor effect of beam reflections in the vapor capillary. This last appearing mainly for high thickness welding (high capillary aspect ratio – low scanning speeds). This assumption validity will be checked after model resolutions. It should be noted that the beam reflections inside the powder bed are also neglected due to the thickness of the bed which is nearly the size of a particle. Nevertheless, the masking effect is naturally considered by the numerical description of heat input. The gas mechanical effect on the liquid free boundary is also neglected due to the poor liquid deformation. It is well known that vapor ejection during laser welding have a strong impact on the stability of the process but as the aspect ratio of the "capillary" (width/thickness) is quite low (close to 1) the vapor, in this case, does not affect so much the fluid behavior [9]. As for the beam reflection this assumption has to be check with the model results. The gas is thus considered only for thermal effects and boundary tracking.

Simulated Geometry

The simulated geometry is composed by two main volumes, the gas on the upper part and the metal on the bottom part (Figure 1). It should be noted, that the powder does not appears yet because it is not considered as a geometrical entity but as an initial condition for the Phase Field problem. This manual initialization allows a computation with a homogeneous mesh and make easier the first steps of resolution.
The illustrated geometry on Figure 1 is *2 mm* long, *500 µm* width and *200 µm* thick (*100 µm* for each phase). These sizes are set in order to simulate an elementary volume representative of a line built. The size of the numerical problem is a real

limitation for this kind of simulation. To reduce it, the length will be downsized to *1 mm* after having validated that the stationary regime is really reached.

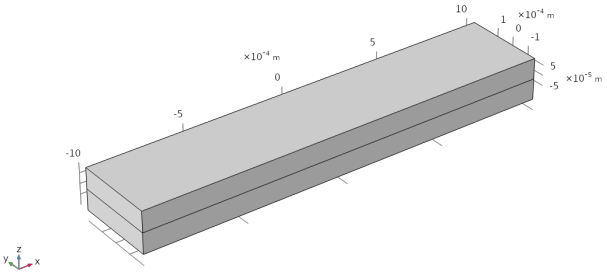

Figure 1: Simulated geometry

Physical Phenomena and Numerical Models

Heat transfers

The heat transfers problem is the resolution of the heat equation:

$$\rho_{\emptyset} c_{p_{\emptyset}}^{eq} \frac{\partial T}{\partial t} + \rho_{\emptyset} c_{p_{\emptyset}} \vec{v}.\overrightarrow{\nabla T} = \vec{\nabla}.\left(\lambda_{\emptyset}\,\overrightarrow{\nabla T}\right) + S.\delta\emptyset$$

With ρ, c_p and λ, respectively the density, the specific heat and the thermal conductivity for each phase (gas and metal). S is the heat input coming from the laser beam and losses due to evaporation. Usually considered as a boundary condition of the metallic part, this term has to be introduced here (due to Phase Field problem) in the bulk and multiplied by a delta function $\delta\emptyset$, the Phase Field variable derivative. In other words, as the interface has a "virtual" thickness and is not a geometrical entity, the source and losses have to be introduced inside the domains but on the Phase Field domain transition zone.

$$S = \varphi_{laser}(t) - \dot{m}L_{vap}$$

The heat source is a classical Gaussian beam:

$$\varphi_{laser}(t) = n_z 2\frac{\alpha(T)P_0}{\pi R_0^2}\exp^{-2\frac{(x-x_0-v_f t)^2+(y-y_0)^2}{R_0^2}}$$

Where n_z is the z component of the normal vector and $\alpha(T)$ is the temperature dependent absorptivity. P_0, R_0 and v_f are respectively the laser power, the beam radius (at $1/e^2$) and the feeding rate. $(x_0 - v_f t)$ and y_0 are the time dependent beam center which moves in the x direction.

$\dot{m}L_{vap}$ is the vaporization lost, calculated from the evaporated mass $\dot{m}$ and the latent heat L_{vap}. The first one comes from the Hertz-Langmuir and Clausius-Clapeyron [10] equations and the second one comes from the literature data.

$$\dot{m} = p_{sat}(T)\sqrt{\frac{M}{2\pi RT}}(1-\beta_r)$$

$$p_{sat} = p_0 \exp^{\frac{ML_v}{R}(\frac{1}{Tv}-\frac{1}{T})}$$

The initial condition is the ambient temperature, set here at *293 K*.

The thermal boundary conditions, in this particular case, have no real impact due to the shape of the problem. As the heat source is assumed far from the boundaries, the local temperature does not change, thus a thermal insulation ($\varphi = 0$) is a good approximation of the real diffusive flux appearing for larger pieces. Only the upper face is slightly different, here the flow can leave the domain, thus the heat transport is allowed.

The radiative lose is neglected here assuming the evaporation flux much larger.

Fluid flows

The fluid calculation is made by solving respectively the momentum and mass conservations for incompressible Newtonian fluids:

$$\rho_{\emptyset}\left[\frac{\partial \vec{v}}{\partial t} + (\vec{v}.\vec{\nabla})\vec{v}\right] = \vec{\nabla}.\left(pI + \mu_{\emptyset}(\vec{\nabla}\vec{v} + (\vec{\nabla}\vec{v})^T\right) + (\sigma\kappa + p_{rec}).\delta\phi$$

$$\vec{\nabla}.\vec{v} = 0$$

ρ still the density and μ is the dynamic viscosity. As previously, the interfacial phenomena; Laplace pressure $\sigma\kappa$ and recoil pressure p_{rec} [10-13], are applied in the domain through a delta function $\delta\phi$.

$$p_{rec} = p_0 + p_{sat}\frac{(1+\beta_r)}{2}$$

β_r is the retro-diffusion coefficient [11].

The initial conditions in velocity and pressure are set to zero.

The boundary conditions are, no slip ($\vec{v} = \vec{0}$) for the metal boundaries and a reference pressure ($p = 0$) for the gas boundaries allowing a potential outflowing.

The flow in the metal is annealed thanks to an "infinite" viscosity appearing with a Heaviside function, for temperature lower than the solidus temperature ($\mu(T) = \mu_0 + 10^6.H(T - T_s)$).

The boundary between metal and gas is not geometrically defined, its definition will thus be done in the next Phase Field section.

Free boundary

Here the free boundary is the whole interface between metal and gas, as well solid as liquid. The method used here is the Phase Field approach simulating a continuous boundary transportation thanks to the Cahn-Hilliard equation:

$$\frac{\partial \phi}{\partial t} + \vec{v}.\overrightarrow{\nabla\phi} = \vec{\nabla}.\gamma\overrightarrow{\nabla G}$$

G is similar to a potential and γ is the mobility determining the time scale of the diffusion phenomena. Both of them are purely numerical parameters in the present case. In the developed formulation, the previous equation can be written in the two following second order PDE solving respectively the Phase Field variable ϕ and the auxiliary variable ψ:

$$\frac{\partial \phi}{\partial t} + \vec{v}.\overrightarrow{\nabla \phi} = \vec{\nabla}.\frac{\gamma\lambda}{\varepsilon^2}\overrightarrow{\nabla \psi}$$

$$\psi = -\vec{\nabla}.\varepsilon^2\overrightarrow{\nabla \phi} + (\phi^2 - 1)\phi + \frac{\varepsilon^2}{\lambda}\frac{\partial f}{\partial \phi}$$

ε is the interface thickness parameter and λ is called the density of mixture energy and link the surface tension to the thickness parameter. $\partial f/\partial \phi$ is an additional energy input.
The Phase Field variable ϕ is thus constrained to take values between -1 and 1 with a continuous transition zone defined from ε through a hyperbolic tangent law.

The boundary settings are mainly a "wetting" condition $\vec{n}.\frac{\gamma\lambda}{\varepsilon^2}\overrightarrow{\nabla \psi} = 0$ and $\vec{n}.\varepsilon^2\overrightarrow{\nabla \phi} = \varepsilon\left|\overrightarrow{\nabla \phi}\right|$. Only the upper boundary is set to an outflow condition.

The initial condition here is the initial shape of the interface. As each particle radius and coordinates come from a previous DEM simulation (Figure 2), authors have manually built a function ϕ_{init} from this input data $p(x_0,y_0,z_0,r_0)$, particle centers and radii.

$$\phi_{init} = N_p - \tanh\left(\frac{z - z_0}{\varepsilon\sqrt{2}}\right) - \sum_{i=0}^{N_p} \tanh\left(\frac{\sqrt{\left(x - x_0^i\right)^2 + \left(y - y_0^i\right)^2 + \left(z - z_0^i\right)^2}}{\varepsilon\sqrt{2}} - {r_0}^i\right)$$

N_p is the total amount of particles, the second term is the flat interface located at $z_0 = 0\ mm$ and the third one is sum of N_p particles p_i located at (x^i_0, y^i_0, z^i_0). The Figure 3 illustrates the "boundary" (ϕ =0) set as initial condition where the powder grains appear.

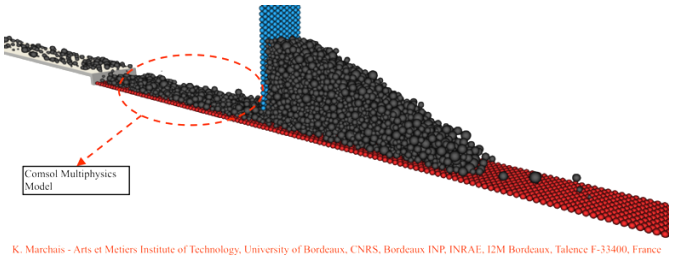

Figure 2: Discrete Element Method model used to feed the FEM model.

Java Programing

The previous Φ_{init} relation is introduced in Comsol thanks Java programming. The built algorithm for powder integration is quite simple:

1. *Import .csv particles data into a Result Table (x_0, y_0, z_0 and r_p)*
2. *Read the total particles amount (N_p)*
3. *Set or read the interface thickness (ε)*
4. *Build a new variable environnement (Var)*
5. *For i is 0 to N-1*
   Build a new variable in Var which is the phase field mathematical formulation of one particle boundary (sphere$_i$)
   Concatenate the string PF formulation of the whole particles (SumSpheres)
6. *Concatenate the whole particles (SumSpheres) with the substrate interface (z_0): Φ_{init}*

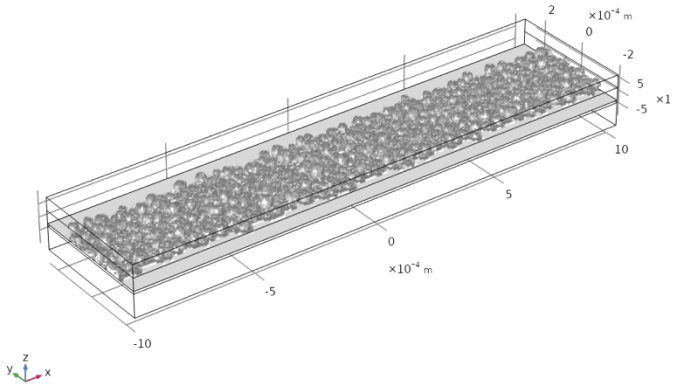

Figure 3: Zero value of the initialized ϕ variable.

The whole Java common steps (geometry, mesh, solving) are kept as built by the soft during the Java transcription. Only links are made between our code and main program (ε, Φ_{init}).

Mesh

As the particles have radii in the range [*4 μm*, *31 μm*], the mesh elements have to be close to the micrometer. Inside the powder zone (Figure 4, upper part) the elements are quadrangular with *2 μm* maximum size and the remaining domains (Figure 4, down part) is meshed with freely growing tetrahedral elements.

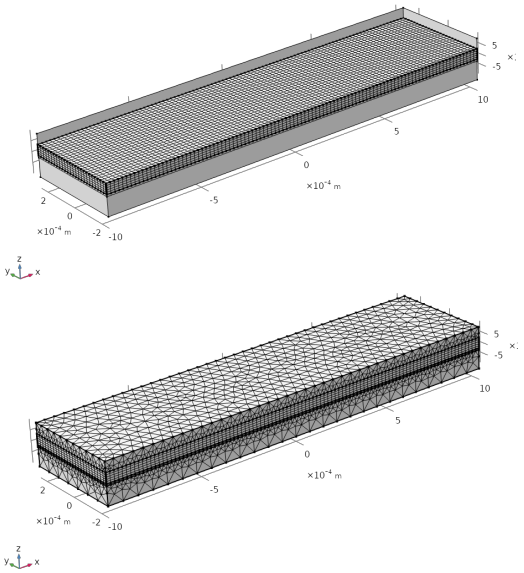

Figure 4: Illustration of the used mesh (up: powder area, down: global mesh)

At this step, this setting produces almost 600,000 DDL to solve.

Results and discussion

Steady state regime time range

At this step, the size of the numerical problem is very large and in order to optimize it, authors assume that the shape of the molten pool can be stationary in less than *2 mm* track length (initial guess).

A test case with poor mesh is thus made for titanium alloy (Ta6V – properties coming from literature [14]) with *200 W* laser power and *50 µm* beam radius. The feeding rate is set at *1 m/s*, a coherent mean value for this process. The results obtained after a day of computation (16 CPU@3.2GHZ) is shown in Figure 5.

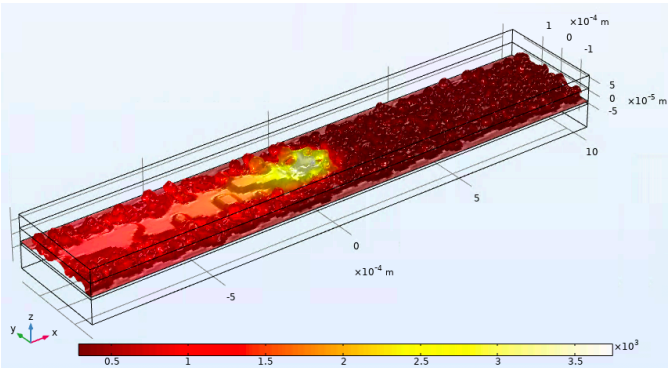

Figure 5: Topological and thermal results at half-track.

In order to reduce the size of the problem, the domain length will be reduced. To avoid analysis error (transient results not reached, for instance), the key dimensions of the molten pool are plotted with the time on Figure 6 (length and width). Two zones can be identified, before *0.4 ms,* the process is highly transient, and after *0.6 ms*, the liquid zone does not change significantly. It should be noted that a maximum appears at *0.5 ms*. This phenomenon is mainly due to the thermal dynamics of the vapor front conjugated to the thermal inertia of the liquid and solid material.

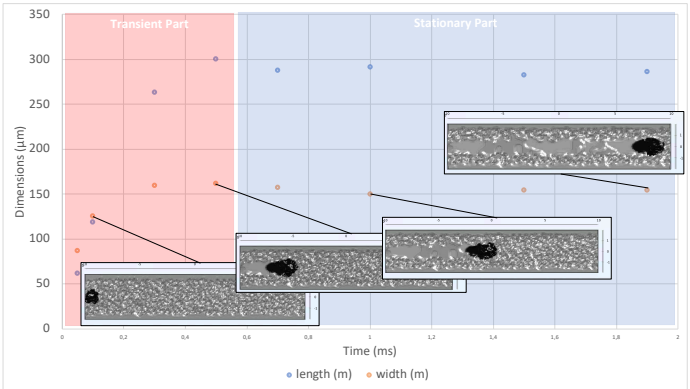

Figure 6: Steady state evaluation with powder bed illustrations (black area is the molten pool).

The Figure 6 illustrates the possibility to reduce the length of the domain from *2 mm* to *1 mm* (Figure 7) without loss of process information. Thus, in the next results part, the geometry is slightly shorter allowing to reduce the characteristic size of the mesh.

Transient analysis

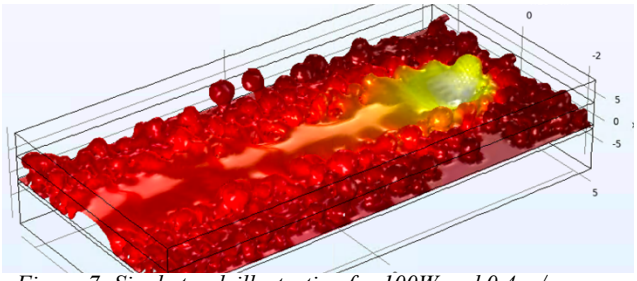

Figure 7: Single track illustration for 100W and 0.4 m/s process parameters.

For LPBF, built quality is very sensitive to the process parameters. As for welding, the laser power and feeding rate can be written as lineic energy (*P/v*). Authors have chosen to change only the velocity between *0.4 m/s* to *1 m/s* and the power is set to *100 W*. Results are shown in Figure 8, where the vaporization zone (white area Figure 8) and molten area are clearly correlated to the lineic energy.

v = 0.4 m/s

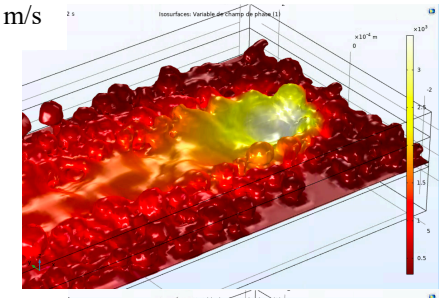

v = 0.6 m/s

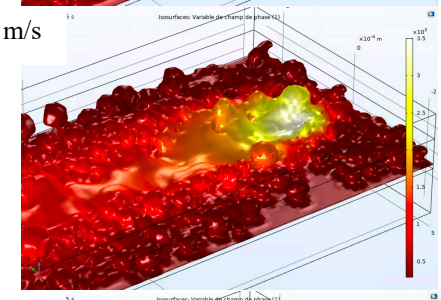

v = 0.8 m/s

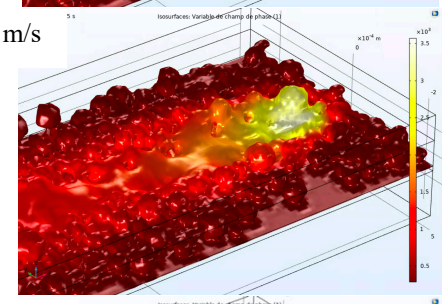

v = 1m/s

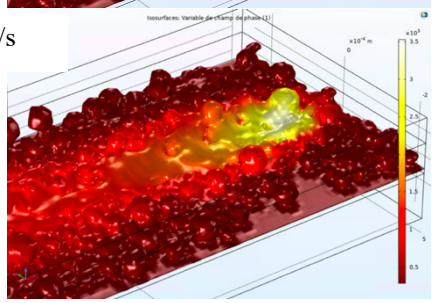

Figure 8: Feed rate effect on molten pool dynamics.

For *0.4 m/s*, i.e. for high lineic energies, the process is quite close to micro laser welding with melting of the substrate, whereas for weak ratio *p/v* (here *1 m/s*) the molten area is much thinner and only the powder seems to be molten. In the last case, the global built (workpiece) will probably have a poor quality due to high number of pores.

With these simulations it is also possible to extract some crucial information as molten pool dimensions or track shapes (Table 1).

Table 1: Molten pool properties and track shapes with the scanning speed.

Scanning speed (m/s)	Length (µm)	Width (µm)	Thickness (µm)	Track shape
0.4	220	78	40	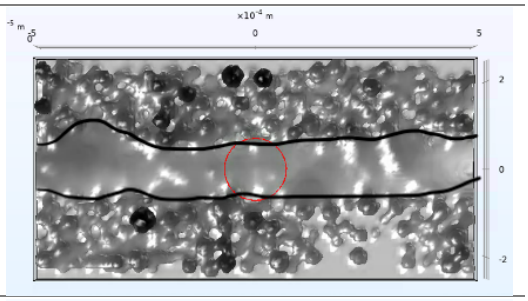
0.6	170	57	30	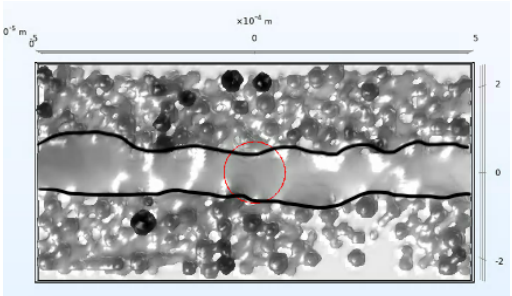
0.8	168	55	24	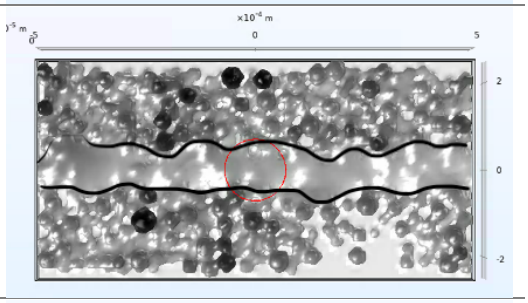
1	175	51	20	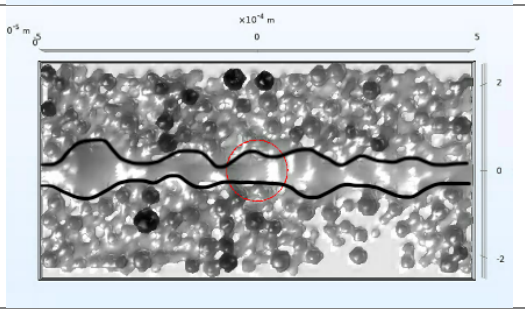

In the Table 1, the liquid zone dimensions tend to evolve as usually in case of laser welding. The length has a non-linear evolution with the scan speed, the width decreases until the size of the beam (here *50 µm* – red circle on pictures) and the thickness decreases until the conduction mode [9].

Nevertheless, measurements are made when the beam is located before the end of the numerical domain as shown in Figure 7 and Figure 8. In the figures of Table 1, the final single-track shapes are shown for the four scanning speeds. Depending on the velocity, one can observe some irregularities appearing for increasing velocities and mainly due to the particle bed irregularities/discontinuity and low linear energy. As the energy density decreases when the velocity increases, irregularities are more sensitive.

At *1 m/s*, they tend to create something similar to the balling observed experimentally when the energy density is too low to melt enough the substrate and the liquid surface tension effect leads the force balance. A second defect is observed at *0.6* and *0.8 m/s* scan speeds, nearly at the half of the piece, one can observe a change in the track directions, leading to a flat v shape of the bead. This effect has already been observed experimentally (Figure 9) and is mainly due to particle size

distribution and its spatial repartition, the molten pool is "attracted" by larger particles.

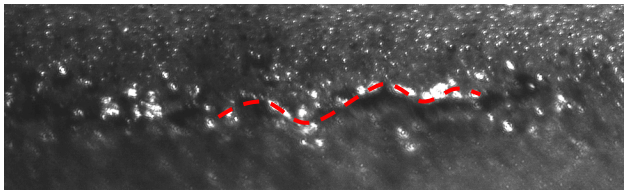

Figure 9: Experimental single-track illustration (dash line: track mean direction).

Assumptions validation

In the first parts of this paper, authors have assumed poor effects of multiple reflections and mechanical shearing between evaporated gas and liquid.
As the results seems to be realistic, we can confirm (or not) these initial guess. The Figure 10 shows middle slices of Φ for the four previous velocities. In the right side of the captures, one can see the liquid deflection due to vaporization process, usually called the "capillary". For each case some information are added. The black dash line (T_f) is tangent to the capillary front surface (where the laser beam is located), the white dash line (T_r) is tangent to the rear surface and the black arrow (n) is the vector normal to T_f.

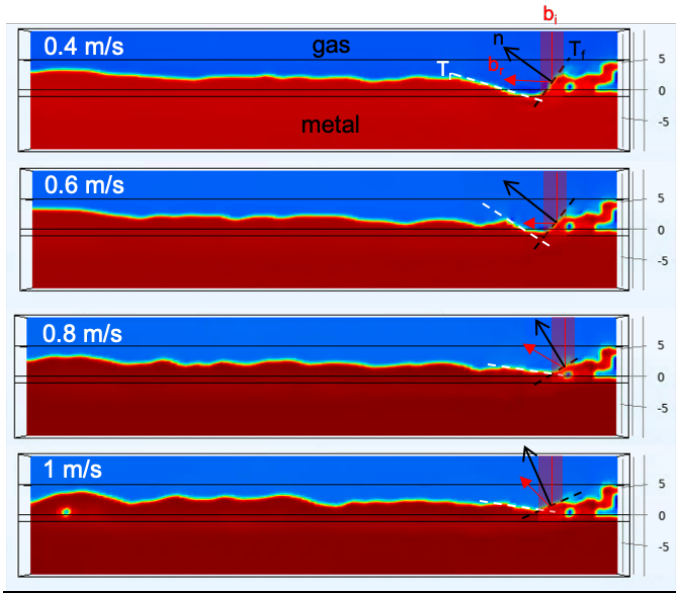

Figure 10: Longitudinal slices of phase field variable.

During the vaporization process, the gas flows out the liquid through the normal vector of the front side. Thus, as there is no intersection between n and T_r it seems to be clear that the vapor does not affect significantly the liquid. In other words, a poor description of gas flow does not affect so much the track shape. That confirms the assumption concerning the gas flow. It should be noted that the angle between n and T_r increase with the velocity and as shown for *0.4 m/s* and *0.6 m/s*, for small velocities (lower than *0.4*), this angle is very small, the assumption is no more suitable.
The beam reflection analysis can be approximated by the geometric schemes shown in the same figure. The incident beam (b_i) is perfectly vertical and is reflected (b_r) on T_f, conserving its angle regarding the normal n. Now, if the reflected beam (b_r) intersect the rear front tangent (T_r), some laser energy will be transported at this intersection point. Here, for *0.4* and *0.6 m/s*, the reflected beams interact with the rear capillary fronts. Thus, our assumption is probably valid only for velocities higher than *0.7* m/s.

It should be added that a porosity appears during the first stage of the 1 m/s single track confirming the lack of substrate melting.

Conclusions

In this paper authors have shown the built of a numerical simulation of additive manufacturing considering the powder bed physically, conversely to common approach using an equivalent powder phase with homogenized properties. This model aims to give accurate information on process defects (pores and instabilities during a workpiece built).

To avoid mesh difficulties due the powder small size and large number of contact points (particle-substrate), an analytical formulation of the interface metal-gas has been done and the transport was computed using an Eulerian formulation (Phase Field). The particle sizes and locations are coming from a previous Discret Element Methode simulation. The powder bed was built and imported in the model through Java Programming making the development easier.
Different geometry and mesh cases have been done, in order to reduce the size of the numerical problem and it has been shown that a domain with *1 mm* length is sufficient here to observe the steady state.
Four scan speed cases have been computed and effects on final tracks appears to be realistic. The slower cases were quite stable, and the faster cases lead to defects observation (variations on track direction, first steps of balling and pores). Indeed, for velocity higher than *1 m/s*, the set laser power (*100 W*) is not sufficient and the substrate does not melt enough.
Finally, two assumptions have been checked. Neglecting the gas shearing on the liquid surface appears to be appropriate for beam velocities higher than *0.4 m/s*. The beam reflections inside the "vapor capillary", also neglected here, seems to be a suitable approximation for scanning speed larger than *0.7 m/s*.

The next stages of this work will concern, accurate experimental validation of the simulation results (temperatures, velocities, track shapes, …).
Moreover, the stable cases founded here are mainly obtained at low scan speeds (or at higher laser power). Thus, our assumptions concerning the gas flow and the beam multiple reflections will not be valid anymore. Current other works are treating these two topics and will be added in this model.

References

1. G. Marion, A Finite Element Model for an Additive Manufacturing Process: Direct Metal Deposition, *International Congress on Applications of Lasers & Electro-Optics* (ICALEO'2014), San Diego (USA), (2014).

2. M. Shakoor, An efficient and parallel level set reinitialization method - application to micromechanics and microstructural evolutions, *Appl. Math. Model*., **39**, 7291–7302 (2015).
3. S. Kolossov, 3D FE simulation for temperature evolution in the selective laser sintering process, *International Journal of Machine Tools & Manufacture*, **44**, 117–123, (2004).
4. M. Dal, A new equivalent approach for additive manufacturing (SLM) numerical simulation, *35th International Congress on Applications of Lasers and Electro-Optics* (ICALEO'2016) San Diego (USA), October 16-20 (2016).
5. Q. Chen, Three-dimensional finite element thermo-mechanical modeling of additive manufacturing by selective laser melting for ceramics materials, *Add. Manu.*, **16**, 124-137 (2017).
6. P Zehner, Wärmeleitfähigkeit von Schüttungen bei mäßigen Temperaturen, *EU Schlünder - Chemie Ingenieur Technik*, Wiley Online Library (1970).
7. M. Rombouts, Photopyroelectric Measurement of Thermal Conductivity of Metallic Powders, *Journal of Applied Physics*, **97,** 024905 (2005).
8. S. Khairallah, Laser powder-bed fusion additive manufacturing: Physics of complex melt flow and formation mechanisms of pores, spatter, and denudation zones, *Acta Materialia*, **108**, 15 36-45 (2016).
9. R. Fabbro, Melt pool and keyhole behaviour analysis for deep penetration laser welding, *Journal of Physics D : Applied Physics,* **43**, 445501 (2010).
10. A.A. Samokhin, Effect of Laser Radiation on Absorbing Condensed Matter, *Nova Science Publishers* (1990).
11. K. Hirano, Experimental determination of temperature threshold for melt surface deformation during laser interaction on iron at atmospheric pressure, *J. Phys. D. Appl. Phys.*, **44**, 435402 (2011).
12. C.J. Knight, Theoretical modeling of rapid surface vaporization with back pressure, *AIAA Journal*, **17**, 5p (1979).
13. A. Matsunawa, The simulation of front keyhole wall dynamics during laser welding, *Journal of Physics D: Applied Physics*, **30**, 798-809 (1997).
14. K.C. Mills, *Recommended values of thermophysical properties for selected commercial alloys*, 211-218, Woodhead Publishing Limited, Cambridge England (2002).